ACS Catalysis

LETTER

pubs.acs.org/acscatalysis

Overcoming the Strong Metal−Support Interaction State: CO Oxidation on TiO_2(110)-Supported Pt Nanoclusters

Simon Bonanni, Kamel Aït-Mansour,* Harald Brune, and Wolfgang Harbich

Institute of Condensed Matter Physics, Ecole Polytechnique Fédérale de Lausanne (EPFL), CH-1015 Lausanne, Switzerland

Supporting Information

ABSTRACT: We combine low-temperature scanning tunneling microscopy and measurements of the catalytic activity to establish a structure−reactivity correlation for the CO oxidation on Pt nanoclusters on rutile TiO_2(110)-(1 × 1). Annealing of the clusters to 1100 K leads to their encapsulation by a reduced titania layer. We present a method how this catalytically passive strong metal−support interaction state can be transformed into a very active one. We believe that our method is of general interest well beyond the presented system.

KEYWORDS: strong metal−support interaction (SMSI), Pt nanoclusters, TiO_2, catalysis, CO oxidation, scanning tunneling microscopy (STM)

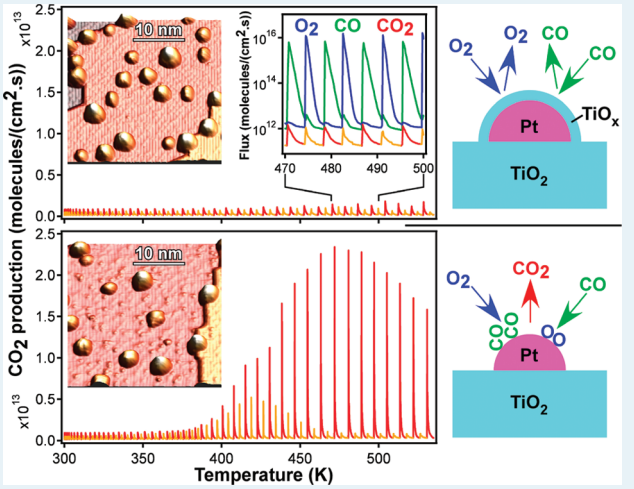

Metal clusters supported on metal oxide surfaces are currently intensively studied as model catalysts to achieve an atomic scale understanding of nanocatalysis.[1,2] Size, crystal structure, chemical composition, and electronic properties of the metal clusters can strongly influence their catalytic activity.[3,4] For instance, the surface of bulk Au is well-known to be catalytically inactive, whereas dispersed Au nanoparticles on oxides exhibit a high catalytic activity for various chemical reactions, for example, for low-temperature CO oxidation.[5−13] Electron charging of Au clusters bound to MgO(001) surface defects strongly influences CO adsorption[14] and CO oxidation.[15−18] In contrast to Au, bulk Pt is known to be an excellent catalyst for a number of reactions, including CO oxidation,[19,20] which justifies its wide use in current industrial catalysts.

However, nanoparticles of Pt, as well as of other group 8−10 noble metals, on TiO_2 lose their H_2 and CO chemisorption capacity when annealed above 700 K.[21] This effect is attributed to a "strong metal-support interaction"[21] (SMSI); the passive state is commonly referred to as the SMSI state.[22−50] Since it severely restricts the practical use of the catalyst, this state has been studied intensively over the last three decades by means of surface-sensitive techniques and for several metals (Pt, Pd, Rh, etc.) on atomically well-defined oxide surfaces such as TiO_2-(110), Fe_3O_4(111), and CeO_2(111), revealing in all cases that the SMSI state is related to an encapsulation of the deposited metal by a reduced thin oxide layer coming from the support during annealing.[24−50] This encapsulation is found to be the cause of the strong decrease in the metal's capacity to adsorb CO.[24−32]

Here, we report on a method to remove the SMSI state for Pt nanoclusters on rutile TiO_2(110)-(1 × 1). We use an ultrahigh vacuum experimental setup[51] combining low-temperature scanning tunneling microscopy (STM)[52] and catalytic measurements. Suboxide-encapsulated Pt clusters are found to be almost inactive in catalytic CO oxidation. As we will show, this SMSI state can be transferred into a very active and thermally stable one, thus overcoming the SMSI limitation.

Figure 1 shows STM images of 25% monolayer (ML) of Pt (1 ML Pt is defined as the Pt(111) atomic surface density = 1.5 × 10^{15} atoms/cm^2) deposited at room temperature on a clean rutile TiO_2(110)-(1 × 1) surface,[53] followed by annealing at 1100 K for 3 h (see the Supporting Information). The overview STM image shows regularly dispersed Pt clusters that appear as bright spots. Images taken at many other locations are very similar and thus reveal that the sample morphology is quite homogeneous, such that spatially integrating catalytic reaction measurements based on mass spectroscopy can safely be related to the shown cluster morphology. The close-up STM image (Figure 1b) shows that the Pt clusters have different apparent sizes and have grown on the bare terraces as well as at the monatomic steps of the TiO_2(110) surface. The bright and dark

Received: January 5, 2011
Revised: February 15, 2011

   dx.doi.org/10.1021/cs200001y | ACS Catal. 2011, 1, 385–389

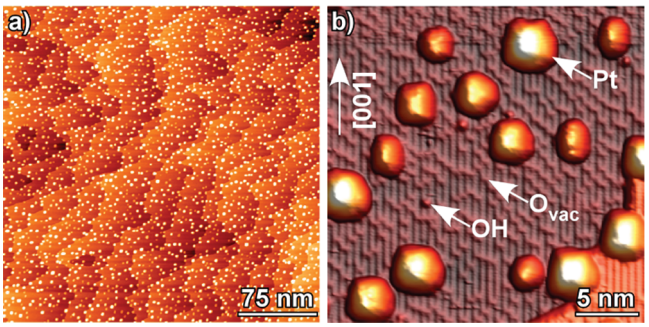

Figure 1. (a) Overview and (b) close-up STM images of 25% ML Pt deposited at room temperature on $TiO_2(110)$-(1 × 1) followed by annealing at 1100 K for 3 h (+1.5 V, 0.1 nA, 80 K).

lines resolved on the bare terraces correspond to [001]-oriented rows of 5-fold-coordinated Ti and bridging O atoms, respectively.[53] In addition, we discern by their apparent heights two types of bright point defects randomly distributed on the oxygen rows. The majority are O vacancies (O_{vac}) appearing with a height of 0.3 Å, and the minority are hydroxyls (OH) with an apparent height of 0.8 Å (see also the Supporting Information). The O_{vac} surface density in the cluster-free surface areas is estimated to 12.5% ML (with respect to the density of the $TiO_2(110)$-(1 × 1) unit cells of 5.2 × 10^{14} cm^{-2}), which means that the surface of the TiO_2 crystal is strongly reduced.[53−56] The STM contrast on the $TiO_2(110)$ terraces is related to the empty states and well-known to be dominated by electronic effects.[53]

Figure 2a displays the CO_2 production on the surface shown in Figure 1 as a function of sample temperature when CO and O_2 reactants are pulsed alternatingly on the sample. To distinguish the product from CO_2 in the residual gas, we dose isotopic $^{13}C^{16}O$ (green) and $^{18}O_2$ (blue in the right insert in Figure 2a) and detect the yield of $^{13}C^{16}O^{18}O$. The flux of the CO_2 product is displayed in red when correlated with the CO pulse and in orange when correlated with the O_2 pulse (right insert in Figure 2a). This CO_2 production is very small. The CO_2 signal is composed of a temperature-independent background coming from the detector walls and a very small increase beyond this above 450 K. The CO_2 production is increased by more than an order of magnitude when this sample is sputtered with argon ions at room temperature and then annealed at 1100 K for 1 h (Supporting Information). As can be seen from comparison of the two STM images shown as insets in Figure 2, the morphology of the catalytically active sample is very similar to the one of the passive sample before the sputter−anneal treatment.

The CO_2 production as a function of temperature in Figure 2b —in particular, its correlation to O_2 at low and CO at high temperature—is reminiscent of Pt being the catalytically active element.[19] Note that Pd(111)[57−59] and Pd nanoclusters on MgO[60] display a similar behavior. The maximum of CO_2 production is observed at ∼470 K and estimated to 0.03 CO_2 per cluster surface Pt atom. This is ∼20 times higher than for the nonsputter-annealed Pt/TiO_2 sample (Figure 2a), estimated after subtraction of the CO_2 background measured at 300 K. It is synchronized with CO reacting with dissociated oxygen chemisorbed on the surfaces of the metal clusters. For temperatures between 370 and 450 K, we observe the coexistence of CO_2 production synchronized with the O_2 dosage. This is due to the oxidation of CO molecules chemisorbed on the clusters. This

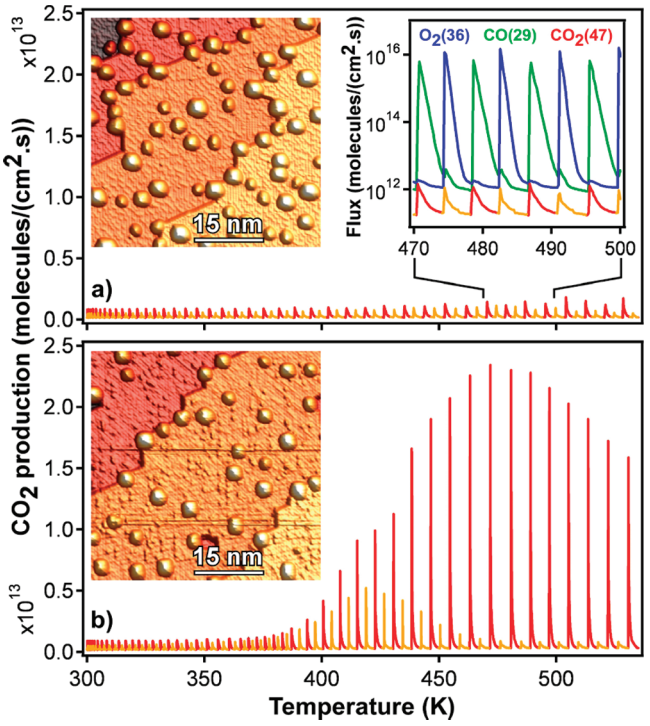

Figure 2. (a) Vanishingly small CO_2 production (red-orange) obtained on the SMSI sample displayed in the left inset upon dosing alternating pulses of O_2 (blue) and CO (green) as shown in the right inset as a function of the sample temperature and time (heating rate 1 K/s, pulse frequency 0.1 Hz). (b) High CO_2 production obtained on the sample displayed in the left inset (same preparation as in panel a), followed by Ar ion sputtering at room temperature and annealing at 1100 K for 1 h). Red and orange colors refer to the CO_2 production synchronized with CO and O_2 pulses, respectively.

CO_2 peak vanishes above 450 K, where CO desorbs and only oxygen remains adsorbed on the cluster surfaces. The fact that there is no CO_2 production beyond the background below 370 K is caused by the Pt clusters being fully covered by CO, leaving no surface sites for the dissociation of O_2 molecules, which is known as CO poisoning of the catalyst.[19,57−60]

A detailed analysis of the cluster morphology of the two differently prepared model catalysts (Figure 2) is presented in the apparent height histograms in Figure 3b and d derived from the STM images of Figure 3a and c, respectively. Both distributions show almost identical average apparent heights of 10.0 and 10.2 Å, respectively. The distributions are similar for large apparent heights; the small ones have a marked peak at 5.5 Å in Figure 3b that disappears in the activated sample (Figure 3d). We estimate the cluster volume from a half-sphere model for the clusters and from their surface densities of 2.7 × 10^{12} and 1.6 × 10^{12} cm^{-2} to be 35% and 19% ML, respectively, which is once above and once below the deposited amount of 25% ML Pt. Although this estimation has to be taken with care, it is indicative of the passive sample indeed presenting an encapsulation layer,[61] whereas this layer is absent—and probably some Pt has been sputtered away—in the active one. A further indication of the presence of a passivation layer in Figure 3a can be derived when attributing the prevailing apparent height of 5.5 Å to a monolayer of Pt covered by Ti suboxide,[61] which is much higher than a clean metal monolayer on TiO_2 (3.5 Å).[62,63] Figure 3 shows that both $Pt/TiO_2(110)$ samples have comparable cluster

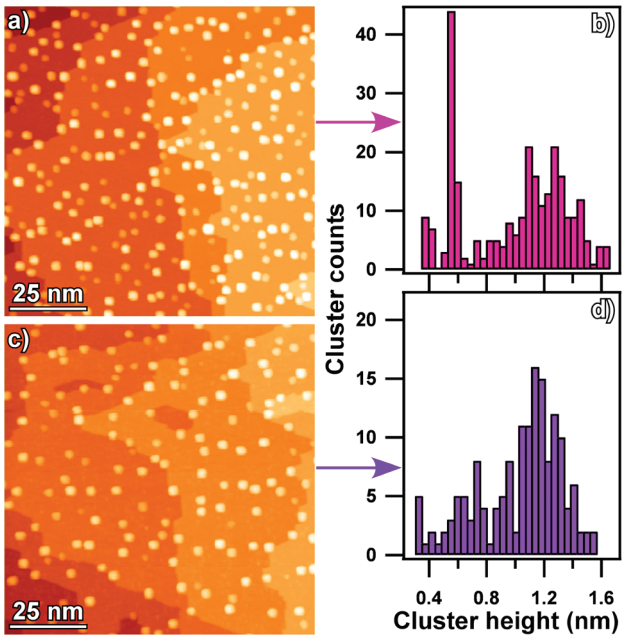

Figure 3. (a) Overview STM image of 25% ML Pt deposited at room temperature on $TiO_2(110)$-(1 × 1) followed by annealing at 1100 K over 3 h. (b) Apparent height distribution of the clusters observed in panel a. (c) Overview STM image of a $Pt/TiO_2(110)$ sample prepared as in panel a and followed by room temperature sputtering and annealing at 1100 K over 1 h. (d) Corresponding apparent height distribution.

sizes such that the large difference in the catalytic activity between the two samples (Figure 2) cannot be attributed to cluster size effects.

We attribute the very low catalytic activity in Figure 2a to the fact that the Pt clusters are encapsulated by a reduced titania layer that forms during the high-temperature treatment, as previously demonstrated and widely accepted in the SMSI literature.[22−50] The encapsulated clusters are characterized by a high thermal stability.[64] The encapsulating layer blocks the active sites of the Pt clusters and therefore passivates them toward the catalytic CO oxidation. The small CO_2 production observed in Figure 2a above 450 K may be caused by a few remaining active Pt sites because it is not observed on clean $TiO_2(110)$ surfaces and its behavior as a function of temperature is characteristic of Pt.

The mechanisms of metal encapsulation on oxides occurring in the SMSI state are complicated and not yet fully understood. One model has been proposed by Fu et al., who argued that the encapsulation is a multistep process and occurs only for metals with larger work function and surface energy as compared with those of the oxide support.[48,49] According to this model, metal encapsulation on TiO_2 requires (i) electron transfer from the oxide to the metal, (ii) the thermally activated outward diffusion of bulk Ti^{3+} interstitials, and finally, (iii) mass transport and migration of a thin oxide layer onto the surface of the metal, driven by a minimization of the surface energy of the system. The case of Pt on reduced $TiO_2(110)$ obeys all these criteria. Indeed, (i) the work function of Pt(111) is higher (by ∼0.7 eV) than the one of $TiO_2(110)$,[48] and electron transfer from Ti^{3+} states of TiO_2-(110) to Pt atoms has been experimentally demonstrated.[65,66] In addition, (ii) the Ti^{3+} depletion from the bulk to the surface of $TiO_2(110)$ occurs for the same reasons as the widely studied oxygen-induced surface reconstruction.[53,56,67−70] Finally, (iii) the surface energy of Pt(111)[48,50] is about 5 times higher than that of $TiO_2(110)$.[71,72] These arguments, together with our reactivity measurements, strongly suggest that high-temperature annealing of Pt on reduced TiO_2 results in the encapsulation of Pt by a reduced titania layer.[33−42]

The high catalytic activity observed in Figure 2b results from sputter removal of the encapsulating suboxide layer from the SMSI Pt/TiO_2 sample. The surprising finding is that the encapsulating layer does not form again when the sputtered $Pt/TiO_2(110)$ sample is annealed to 1100 K. In addition to removing the encapsulation from the thermally stable Pt clusters,[64] ion sputtering also increases the reduction state of the cluster-free surface regions by preferentially depleting them of oxygen.[53] Annealing of oxygen-depleted TiO_2 surfaces above 700 K under ultrahigh vacuum restores the stoichiometry by the diffusion of Ti cations from the surface to the bulk of the crystal.[73] This is the case on Pt-free surface regions that appear in STM as clean $TiO_2(110)$-(1 × 1) with close to bulk stoichiometry (see Supporting Information). During the annealing of the sputtered sample to 1100 K, the diffusion direction of the Ti cations in the Pt-free surface regions is thus opposite to the one of the encapsulation process. In addition, the sputter-induced surface Ti cations diffuse into the bulk of the TiO_2 crystal rather than onto the Pt clusters.

We note that Rh and Pd particle encapsulation does occur if the metal is vapor-deposited on presputtered $TiO_2(110)$ surfaces that are then annealed to high temperatures.[32,48] This indicates that the absence of encapsulation in the case of our sputter-annealed $Pt/TiO_2(110)$ sample is due to the fact that the ion-sputtering treatment is performed after, not before, the clusters are formed and encapsulated. Due to the mechanisms outlined above occurring during the encapsulation, the interface between the metal clusters and the oxide support is expected to be modified by the encapsulation. This encapsulation-induced interface modification is a possible reason why the encapsulation process is self-limited to suboxide thicknesses of only one or two ML, as reported in the case of different metals on various oxide surfaces.[24−50] The self-limitation of the encapsulation is supported in our catalytic measurements by the small CO_2 production (Figure 2a) on the encapsulated Pt clusters, which likely still expose some active Pt sites at their surfaces, even after 3 h of heating at 1100 K. Therefore, one can understand that, if the suboxide layer encapsulating the metal clusters is removed, its reformation by subsequent high-temperature annealing is quenched. This gives rise to the highly active and thermally stable Pt clusters characterized in Figure 2b. In line with the metal-oxide-interface-based interpretation proposed here, we note that Nb doping of the near-surface region of TiO_2 also quenches the encapsulation of Pt during annealing.[50] To better understand the reasons for the metal encapsulation quenching, further investigations are necessary.

In conclusion, we have reported a sputter−anneal procedure that transfers Pt nanoclusters on $TiO_2(110)$-(1 × 1) from their almost inert SMSI state to a catalytically active and thermally stable one for CO oxidation. The procedure prevents the encapsulation of the Pt clusters by a thin, reduced titania layer, which usually forms by high-temperature treatment of Pt/TiO_2 and is known to be responsible for the catalytic passivity of the metal clusters. This procedure can in principle be applied to other (ultra)high-vacuum-prepared SMSI systems and to other catalytic reactions.

dx.doi.org/10.1021/cs200001y |*ACS Catal.* 2011, 1, 385–389

■ ASSOCIATED CONTENT

Supporting Information. Experimental details, STM images of the clean $TiO_2(110)$-(1×1) surface, catalytic CO oxidation on $Pt/TiO_2(110)$-(1×1) after deposition at room temperature, further STM images of $Pt/TiO_2(110)$, determination of the gas amounts, simulation of the CO oxidation. This material is available free of charge via the Internet at http://pubs.acs.org.

■ AUTHOR INFORMATION

Corresponding Author
*E-mail: kamel.ait-mansour@epfl.ch.

■ ACKNOWLEDGMENT

Financial support by the Swiss National Science Foundation is gratefully acknowledged. We thank Claude Henry and Hassan Sadeghi for helpful discussions.

■ REFERENCES

(1) Henry, C. R. *Surf. Sci. Rep.* **1998**, *31*, 231–325.
(2) Henry, C. R. *Prog. Surf. Sci.* **2005**, *80*, 92–116.
(3) Campbell, C. T. *Surf. Sci. Rep.* **1997**, *27*, 1–111.
(4) Cho, A. *Science* **2003**, *299*, 1684–1685.
(5) Haruta, M. *Catal. Today* **1997**, *36*, 153–166.
(6) Haruta, M.; Tsubota, S.; Kobayashi, T.; Kageyama, H.; Genet, M. J.; Delmon, B. *J. Catal.* **1993**, *144*, 175–192.
(7) Valden, M.; Lai, X.; Goodman, D. W. *Science* **1998**, *281*, 1647–1650.
(8) Choudhary, T. V.; Goodman, D. W. *Appl. Catal., A* **2005**, *291*, 32–36.
(9) Campbell, C. T. *Science* **2004**, *306*, 234–235.
(10) Lopez, N.; Nørskov, J. K. *J. Am. Chem. Soc.* **2002**, *124*, 11262–11263.
(11) Kim, T. S.; Stiehl, J. D.; Reeves, C. T.; Meyer, R. J.; Mullins, C. B. *J. Am. Chem. Soc.* **2003**, *125*, 2018–2019.
(12) Lee, S.; Fan, C.; Wu, T.; Anderson, S. L. *J. Am. Chem. Soc.* **2004**, *126*, 5682–5683.
(13) Lee, S.; Fan, C.; Wu, T.; Anderson, S. L. *J. Chem. Phys.* **2005**, *123*, 124710-1–124710-13.
(14) Lin, X.; Yang, B.; Benia, H.-M.; Myrach, P.; Yulikov, M.; Aumer, A.; Brown, M. A.; Sterrer, M.; Bondarchuk, O.; Kieseritzky, E.; Rocker, J.; Risse, T.; Gao, H.-J.; Nilius, N.; Freund, H.-J. *J. Am. Chem. Soc.* **2010**, *132*, 7745–7749.
(15) Sanchez, A.; Abbet, S.; Heiz, U.; Schneider, W.-D.; Ha1kkinen, H.; Barnett, R. N.; Landman, U. *J. Phys. Chem. A* **1999**, *103*, 9573–9578.
(16) Yoon, B.; Häkkinen, H.; Landman, U.; Wörz, A. S.; Antonietti, J.-M.; Abbet, S.; Judai, K.; Heiz, U. *Science* **2005**, *307*, 403–407.
(17) Arenz, M.; Landman, U.; Heiz, U. *ChemPhysChem* **2006**, *7*, 1871–1879.
(18) Roldán, A.; Ricart, J. M.; Illas, F.; Pacchioni, G. *J. Phys. Chem. C* **2010**, *114*, 16973–16978.
(19) Campbell, C. T.; Ertl, G.; Kuipers, H.; Segner, J. *J. Chem. Phys.* **1980**, *73*, 5862–5873.
(20) Wintterlin, J.; Völkening, S.; Janssens, T. V. W.; Zambelli, T.; Ertl, G. *Science* **1997**, *278*, 1931–1934.
(21) Tauster, S. J.; Fung, S. C.; Garten, R. L. *J. Am. Chem. Soc.* **1978**, *100*, 170–175.
(22) Tauster, S. J. *Acc. Chem. Res.* **1987**, *20*, 389–394.
(23) Haller, G. L.; Resasco, D. E. *Adv. Catal.* **1989**, *36*, 173–235.
(24) Sadeghi, H. R.; Henrich, V. E. *Appl. Surf. Sci.* **1984**, *19*, 330–340.
(25) Sadeghi, H. R.; Henrich, V. E. *J. Catal.* **1988**, *109*, 1–11.
(26) Bowker, M.; Stone, P.; Morrall, P.; Smith, R.; Bennett, R.; Perkins, N.; Kvon, R.; Pang, C.; Fourre, E.; Hall, M. *J. Catal.* **2005**, *234*, 172–181.
(27) Bowker, M.; Stone, P.; Bennett, R.; Perkins, N. *Surf. Sci.* **2002**, *497*, 155–165.
(28) Bowker, M.; Fourré, E. *Appl. Surf. Sci.* **2008**, *254*, 4225–4229.
(29) Bowker, M. *Phys. Chem. Chem. Phys.* **2007**, *9*, 3514–3521.
(30) Qin, Z.-H.; Lewandowski, M.; Sun, Y.-N.; Shaikhutdinov, S.; Freund, H.-J. *J. Phys. Chem. C* **2008**, *112*, 10209–10213.
(31) Qin, Z.-H.; Lewandowski, M.; Sun, Y.-N.; Shaikhutdinov, S.; Freund, H.-J. *J. Phys.: Condens. Matter* **2009**, *21*, 134019-1–134019-6.
(32) Berkó, A.; Ulrych, I.; Prince, K. C. *J. Phys. Chem. B* **1998**, *102*, 3379–3386.
(33) Dulub, O.; Hebenstreit, W.; Diebold, U. *Phys. Rev. Lett.* **2000**, *84*, 3646–3649.
(34) Jennison, D. R.; Dulub, O.; Hebenstreit, W.; Diebold, U. *Surf. Sci.* **2001**, *492*, L677–L687.
(35) Belton, D. N.; Sun, Y.-M.; White, J. M. *J. Phys. Chem.* **1984**, *88*, 5172–5176.
(36) Sun, Y.-M.; Belton, D. N.; White, J. M. *J. Phys. Chem.* **1986**, *90*, 5178–5182.
(37) Pesty, F.; Steinrück, H.-P.; Madey, T. E. *Surf. Sci.* **1995**, *339*, 83–95.
(38) Haller, G. L. *J. Catal.* **2003**, *216*, 12–22.
(39) Park, J. B.; Ratliff, J. S.; Ma, S.; Chen, D. A. *J. Phys. Chem. C* **2007**, *111*, 2165–2176.
(40) Park, J. B.; Conner, S. F.; Chen, D. A. *J. Phys. Chem. C* **2008**, *112*, 5490–5500.
(41) Ozturk, O.; Park, J. B.; Ma, S.; Ratliff, J. S.; Zhou, J.; Mullins, D. R.; Chen, D. A. *Surf. Sci.* **2007**, *601*, 3099–3113.
(42) Bardi, U.; Tamura, K.; Nihei, Y. *Catal. Lett.* **1989**, *3*, 117–128.
(43) Sadeghi, H. R.; Henrich, V. E. *J. Catal.* **1984**, *87*, 279–282.
(44) Bennett, R. A.; Pang, C. L.; Perkins, N.; Smith, R. D.; Morrall, P.; Kvon, R. I.; Bowker, M. *J. Phys. Chem. B* **2002**, *106*, 4688–4696.
(45) Bennett, R. A.; Stone, P.; Bowker, M. *Catal. Lett.* **1999**, *59*, 99–105.
(46) Bernal, S.; Calvino, J. J.; Cauqui, M. A.; Gatica, J. M.; López Cartes, C.; Pérez Omil, J. A.; Pintado, J. M. *Catal. Today* **2003**, *77*, 385–406.
(47) Zhou, Y.; Perket, J. M.; Zhou, J. *J. Phys. Chem. C* **2010**, *114*, 11853–11860.
(48) Fu, Q.; Wagner, T.; Olliges, S.; Carstanjen, H.-D. *J. Phys. Chem. B* **2005**, *109*, 944–951.
(49) Fu, Q.; Wagner, T. *Surf. Sci. Rep.* **2007**, *62*, 431–498.
(50) Gao, Y.; Liang, Y.; Chambers, S. A. *Surf. Sci.* **1996**, *365*, 638–648.
(51) Jödicke, H.; Schaub, R.; Bhowmick, A.; Monot, R.; Buttet, J.; Harbich, W. *Rev. Sci. Instrum.* **2000**, *71*, 2818–2828; see also Bonanni, S.; Aït-Mansour, K.; Hugentobler, M.; Brune, H.; Harbich, W. *Eur. Phys. J. D*, in press.
(52) All STM images have been measured in the constant-current mode (sample bias = +1.5 V, tunneling current = 0.1 nA) at a sample temperature of 80 K, and they have been processed with the WSxM software: Horcas, I.; Fernández, R.; Gómez-Rodríguez, J. M.; Colchero, J.; Gómez-Herrero, J.; Baro, A. M. *Rev. Sci. Instrum.* **2007**, *78*, 013705-1–013705-8.
(53) Diebold, U. *Surf. Sci. Rep.* **2003**, *48*, 53–229 and references therein.
(54) Wendt, S.; Sprunger, P. T.; Lira, E.; Madsen, G. K. H.; Li, Z.; Hansen, J. Ø.; Matthiesen, J.; Blekinge-Rasmussen, A.; Lægsgaard, E.; Hammer, B.; Besenbacher, F. *Science* **2008**, *320*, 1755–1759.
(55) Yim, C. M.; Pang, C. L.; Thornton, G. *Phys. Rev. Lett.* **2010**, *104*, 036806-1–036806-4.
(56) Zhang, Z.; Lee, J.; Yates, J. T., Jr.; Bechstein, R.; Lira, E.; Hansen, J. Ø.; Wendt, S.; Besenbacher, F. *J. Phys. Chem. C* **2010**, *114*, 3059–3062.
(57) Engel, T.; Ertl, G. *Chem. Phys. Lett.* **1978**, *54*, 95–98.
(58) Engel, T.; Ertl, G. *J. Chem. Phys.* **1978**, *69*, 1267–1281.

(59) Conrad, H.; Ertl, G.; Küppers, J. *Surf. Sci.* **1978**, *76*, 323.
(60) Kunz, S.; Schweinberger, F. F.; Habibpour, V.; Röttgen, M.; Harding, C.; Arenz, M.; Heiz, U. *J. Phys. Chem. C* **2010**, *114*, 1651–1654.
(61) Sedona, F.; Rizzi, G. A.; Agnoli, S.; Llabrés i Xamena, F. X.; Papageorgiou, A.; Ostermann, D.; Sambi, M.; Finetti, P.; Schierbaum, K.; Granozzi, G. *J. Phys. Chem. B* **2005**, *109*, 24411–24426.
(62) Isomura, N.; Wu, X.; Watanabe, Y. *J. Chem. Phys.* **2009**, *131*, 164707-1–164707-4.
(63) Isomura, N.; Wu, X.; Hirata, H.; Watanabe, Y. *J. Vac. Sci. Technol. A* **2010**, *28*, 1141–1144.
(64) Naitabdi, A.; Behafarid, F.; Roldan Cuenya, B. *Appl. Phys. Lett.* **2009**, *94*, 083102-1–083102-3.
(65) Schierbaum, K. D.; Fischer, S.; Torquemada, M. C.; de Segovia, J. L.; Román, E.; Martín-Gago, J. A. *Surf. Sci.* **1996**, *345*, 261–273.
(66) Fischer, S.; Schneider, F.; Schierbaum, K. D. *Vacuum* **1996**, *47*, 1149–1152.
(67) Onishi, H.; Iwasawa, Y. *Phys. Rev. Lett.* **1996**, *76*, 791–794.
(68) Onishi, H.; Iwasawa, Y. *Surf. Sci.* **1994**, *313*, L783–L789.
(69) Bennett, R. A.; Stone, P.; Price, N. J.; Bowker, M. *Phys. Rev. Lett.* **1999**, *82*, 3831–3834.
(70) Li, M.; Hebenstreit, W.; Gross, L.; Diebold, U.; Henderson, M. A.; Jennison, D. R.; Schultz, P. A.; Sears, M. P. *Surf. Sci.* **1999**, *437*, 173–190.
(71) Kiejna, A.; Pabisiak, T.; Gao, S. W. *J. Phys.: Condens. Matter* **2006**, *18*, 4207–4217.
(72) Harris, L. A.; Quong, A. A. *Phys. Rev. Lett.* **2004**, *93*, 086105-1–086105-4.
(73) Henderson, M. A. *Surf. Sci.* **1999**, *419*, 174–187.

SUPPORTING INFORMATION

Overcoming the Strong Metal-Support Interaction State: CO Oxidation on TiO_2(110)-Supported Pt Nanoclusters

Simon Bonanni, Kamel Aït-Mansour,* Harald Brune, and Wolfgang Harbich

Institute of Condensed Matter Physics, Ecole Polytechnique Fédérale de Lausanne (EPFL), CH-1015 Lausanne, Switzerland

*E-mail: kamel.ait-mansour@epfl.ch

1) Experiment

Experiments have been carried out in an ultra-high vacuum system containing two main chambers connected to each other by a transfer chamber. One is for the preparation of sample surfaces by ion sputtering and annealing, for the deposition of mass-selected metal clusters[1a] and for catalytic reaction measurements. These are taken out with a home-built detector (sniffer)[1b] minimizing the influence of reactions taking place elsewhere than on the sample and enabling to dose gas pulses and to study the reaction kinetics with ms temporal resolution. The other chamber houses a home-built low-temperature scanning tunneling microscope (STM) operated in the present study at 80 K. The base pressures in the preparation-catalysis and STM chambers are typically in the low 10^{-10} and 10^{-11} mbar ranges, respectively. The STM images presented in this paper have been measured in the constant-current mode (tunneling voltage = +1.5 V, tunneling current = 0.1 nA), the stated voltage refers to the electric potential of the sample with respect to the tip. The STM tips have been electrochemically etched from a tungsten wire. The STM images have been processed with the WSxM software.[2]

The rutile TiO_2(110) single-crystal substrate (6.0 mm × 4.2 mm, thickness ≈ 3 mm) used in this work has been purchased from MTI Corporation. It was mounted in a transferable molybdenum sample holder, where the back side of the sample was supported on a tantalum plate. The clean TiO_2(110)-(1×1) surface has been prepared by repeated cycles of Ar-ion sputtering (150 nA, 1 kV, 13 hours) at room temperature (RT) followed by annealing (through electron-beam bombardment of the supporting tantalum plate) at 1100 K for one hour. The temperature was controlled by a chromel-alumel thermocouple touching the back side of the crystal. Sputtering-annealing cycles reduce the TiO_2(110) crystal by producing point defects such as bulk Ti^{3+} interstitials, as well as bulk and surface O vacancies. These defects introduce electronic states in the TiO_2 band gap, which makes STM measurements possible.[3] The reduction of the TiO_2(110) crystal is accompanied by a color change from transparent to dark blue, which fingerprints the presence of a number of color centers associated with bulk defects.[3] The as-reduced TiO_2 crystal has been used as substrate for the Pt clusters.

Pt_1^+ ions were deposited with a kinetic energy of 7 eV by means of the mass-selected cluster source on the clean TiO_2(110)-(1×1) surface kept at RT. In order to obtain the coverage of 25% monolayer (ML), the sample has been exposed to a Pt_1^+ current of 4 nA for 65 min. After controlling the surface morphology with the STM, the sample was annealed at 1100 K during three hours. Subsequently, the STM investigations and catalytic CO oxidation measurements presented in the paper have been carried out. The second and catalytically active Pt/TiO_2(110) sample has been prepared exactly as the first, but in addition the sample has been sputtered (30 nA, 1 kV, 13

hours) at RT and subsequently annealed at 1100 K for one hour.

In order to determine the real temperature of the sample surface during the catalytic CO oxidation measurements carried out with a heating rate of 1 K/s, the temperature measured by the thermocouple has been calibrated by thermal desorption spectroscopy measurements of water (first, second, and multilayers) and oxygen on the TiO_2(110)-(1×1) surface. The measured water and oxygen desorption temperatures have been compared with values available in literature[4,5] to determine a calibration function which has been used to deduce the real temperature of the sample as indicated in the paper.

2) STM measurements of the clean TiO_2(110)-(1×1) surface

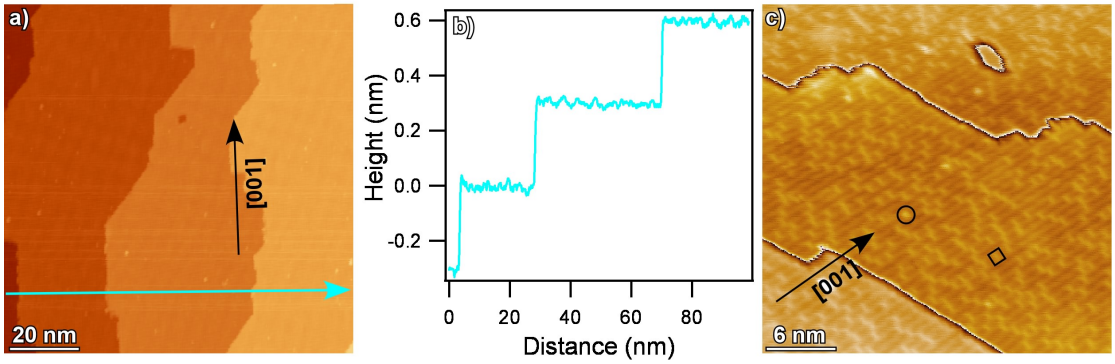

Figure S1. *(a) Overview STM image of the clean TiO_2(110)-(1×1) surface showing monatomic steps. (b) Height profile along the cyan line indicated in (a) showing that the TiO_2 steps have an apparent height of 3.2 Å. (c) Close-up STM image revealing the [001]-oriented titanium (bright) and oxygen (dark) rows of the TiO_2(110)-(1×1) terraces, as well as point defects which are mostly O_{vac} (one of them is highlighted by a square) with few OH (circle). Each terrace has been color-coded individually in order to enhance the contrast.*

Figure S1 shows STM images of the clean TiO_2(110)-(1×1) surface prepared as outlined above. Figure S1a shows large terraces with widths exceeding 30 nm, separated by steps with a height of 3.2 Å, which agrees well with the value of 3.24 Å expected for monatomic steps from the rutile crystal structure. A high resolution STM image is shown in Figure S1c. On the bare terraces it reveals bright and dark lines corresponding to the [001]-oriented rows of fivefold coordinated Ti and bridging O atoms, respectively.[3] A number of point defects are also seen, which are mostly O vacancies (O_{vac}, represented with a square and appearing 0.3 Å higher than the O rows) and some hydroxyls (OH, represented with a circle and having an apparent height of 0.8 Å), the latter resulting from the dissociation of residual gas water molecules at O_{vac} sites.[6] The O_{vac} density estimated from Figure S1c amounts to 9.0% ML (here, two OH are counted as a single O_{vac} (see reference 6)), with the ML definition as in the manuscript. We find that the O_{vac} concentration is rather inhomogeneous over the crystal, and on the same sample there are terraces with 5.4% ML. We derive a mean value of (7 ± 1) % ML. This value is smaller than the one after Pt deposition and cluster formation, as outlined in the manuscript and below; however, it is indicative of a strongly reduced TiO_2 crystal,[3,6-8] in agreement with its dark blue color.

3) Catalytic CO oxidation on $Pt/TiO_2(110)$-(1×1) after deposition at RT

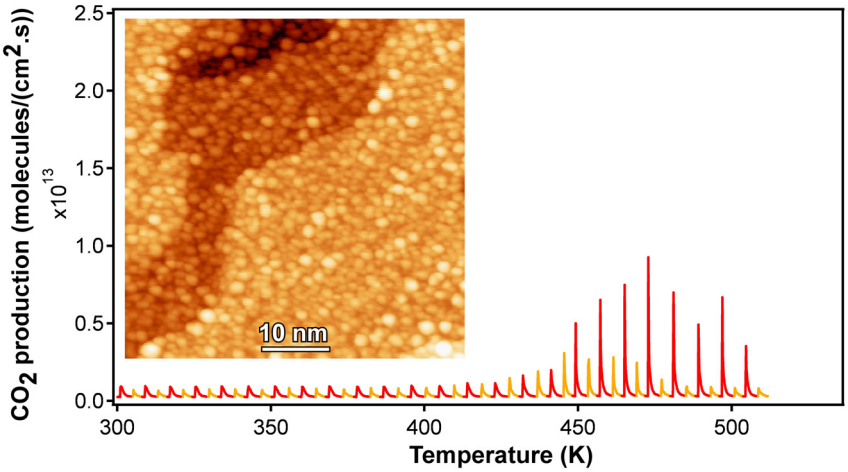

Figure S2. *CO_2 production obtained on 25% ML $Pt/TiO_2(110)$-(1×1) after RT deposition. The surface morphology of the sample is shown in the inset STM image.*

Figure 2S shows that the $Pt/TiO_2(110)$-(1×1) sample after deposition at RT (see the inset STM image for the surface morphology) is much more active for the catalytic CO oxidation than after annealing it at 1100 K, which demonstrates that Pt encapsulation takes place only after the high-temperature treatment.

4) STM measurements of Pt nanoclusters on $TiO_2(110)$-(1×1)

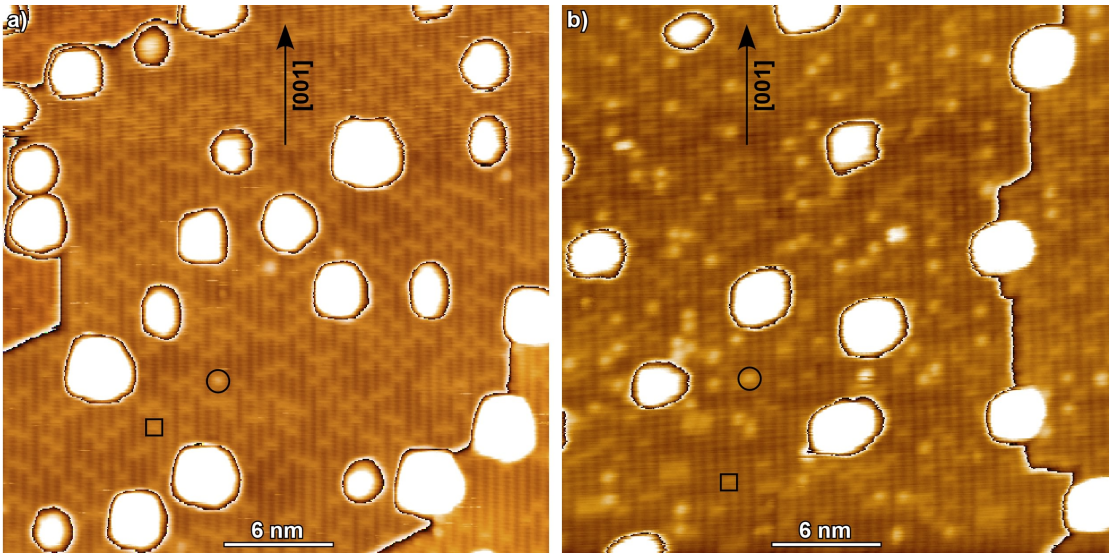

Figure S3. *(a) High resolution STM image of 25% ML Pt deposited at RT on $TiO_2(110)$-(1×1) followed by annealing at 1100 K during three hours. (b) STM image of a $Pt/TiO_2(110)$ sample prepared as in (a) and followed by RT sputtering and annealing at 1100 K during one hour. Squares and circles refer to O_{vac} and OH, respectively. In both STM images, the heights of the $TiO_2(110)$ steps have been subtracted in order to enhance the contrast related to the atomic features on the bare terraces.*

Figure S3a shows an STM image of the same sample as the one in Figures 1 and 2a inset of the

manuscript. The clusters are localized on the bare terraces as well as at the steps of the TiO_2(110) surface. The terraces cover 85% of the image and their defect structure is clearly resolved enabling to estimate the reduction state after cluster growth. We find an O_{vac} concentration of 12.5% ML, which is almost twice as much as on the clean TiO_2(110)-(1×1) surfaces. The higher O_{vac} concentration is expected due to the longer annealing. This further reduces the surface due to additional O desorption, and in addition O can diffuse onto the Pt nanoparticles and participate in their titania encapsulation.

Figure S3b shows for comparison the surface where the SMSI state has been removed in the way described in the paper. The surface covered by Pt clusters is slightly smaller such that the terraces cover 92% of the image. Again, the point defects on the terraces are resolved. The OH species are much more abundant; however the O_{vac} concentration is with 7.2% ML identical to the one of the clean surface. Therefore the terraces are significantly more reduced on the SMSI sample while the catalytically active one shows the same reduction state as the clean TiO_2 surface.

5) Determination of the gas amounts dosed onto, and coming off, the sample

For a quantitative analysis of the ion current measured by the sniffer in terms of number of gas molecules dosed onto, and coming off, the sample per unit time and surface area, two calibrations have been performed. (i) The calibration of the dose requires to establish a relation between the partial pressure in the sniffer and the measured ion current. This has been achieved by having no sample in front of the sniffer and not pumping it, while backfilling the main (preparation-catalysis) chamber with stepwise increasing Ar pressures. Under these conditions the Ar pressure inside the sniffer equals the one in the main chamber read out by a calibrated gauge. (ii) For the calibration of the flux of desorbing species, we have performed thermal desorption spectroscopy of CO and H_2O on TiO_2(110)-(1×1) with the usual operation mode where the sample is close to the sniffer entrance in order to minimize gas exchange with the main chamber, and the sniffer has been pumped differentially. The calibration has been derived by comparing the integrals of the desorption peaks of both molecules with those found in the literature.[5,9]

6) Simulation of the CO oxidation on a Pt(111) surface

In the simulation, as in experiment, the reactants are pulsed with a delay and associated with CO and O coverages on a Pt(111) surface. These coverages vary with time and hence with temperature as given by the following coupled differential equations:

$$\frac{d\theta_{CO}}{dt} = -\nu_{CO}.\theta_{CO}.e^{\frac{-E_{CO}(\theta_{CO})}{k_B.T(t)}} + P_{CO}(t).(1-\theta_{CO}) - A.\theta_{CO}.\theta_O \qquad (1)$$

$$\frac{d\theta_O}{dt} = -\nu_O.\theta_O{}^2.e^{\frac{-E_O(\theta_O)}{k_B.T(t)}} + P_O(t).(1-\theta_O-\theta_{CO})^2 - A.\theta_{CO}.\theta_O \qquad (2)$$

The first terms on the right side of equations 1 and 2 describe the desorption, where θ_i (i = CO or O) are the coverages, ν_i the attempt frequencies, and $E_i(\theta_i)$ the possibly coverage-dependent adsorption energies of CO and O. The second terms describe the adsorption, which is proportional to $P_i(t)$, which itself is proportional to the product of the pulse intensity and the sticking factor. This term is proportional to the number of free adsorption sites for CO, and proportional to the square of this number for O_2 since its adsorption is dissociative. Since adsorbed oxygen does not hinder the

reaction while adsorbed CO does, we consider an oxygen-occupied site to be a free one for CO adsorption, but a CO-occupied site is an occupied one for oxygen adsorption. The last terms in the two equations account for the adsorbed CO and O consumption due to the CO_2 production. They are given by the product of the coverages and a reaction speed A which is assumed to be constant. The CO_2 molecules are supposed to desorb immediately after they are produced, i.e., there is no CO_2-occupied site on the surface. T, t, and k_B (1.38×10^{-23} J/K) are temperature, time, and the Boltzmann constant, respectively. The values used in the simulation are: $\nu_{CO} = \nu_O = 10^{13}$ s^{-1}, $E_{CO}(\theta_{CO}) = (1.22 - 0.25 \times \theta_{CO})$ eV, and $E_O(\theta_O) = 2.17$ eV, both adsorption energies being in agreement with literature data.[10]

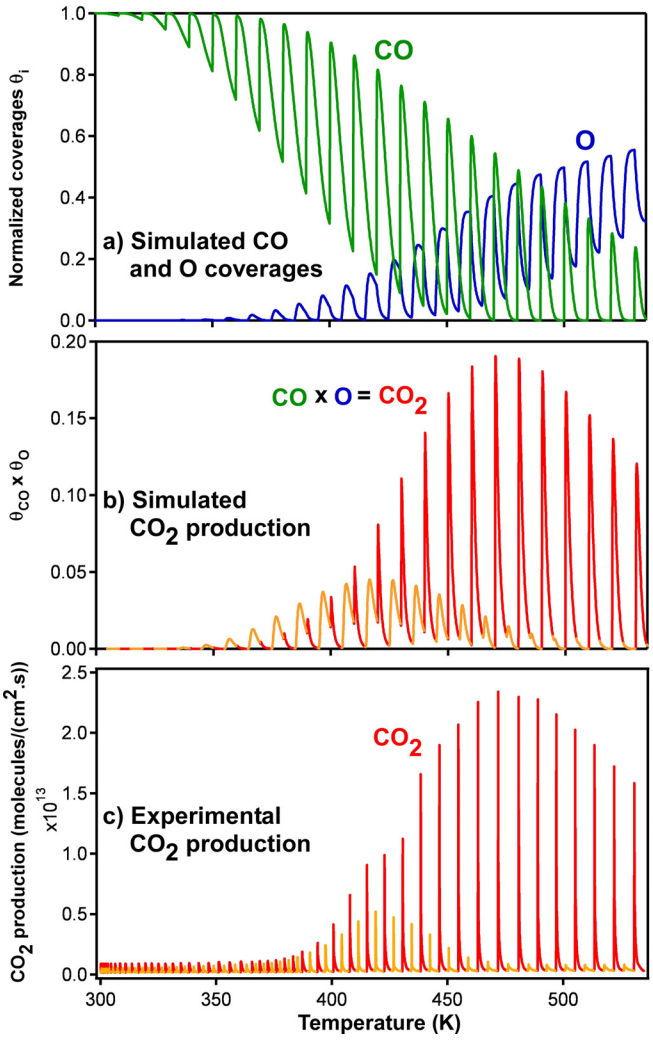

Figure S4. *(a) Simulated CO and O coverages on a Pt(111) surface as a function of temperature. (b) Simulated CO_2 production calculated as the product of the CO and O coverages shown in (a). The CO_2 production peaks synchronized with oxygen peaks are shown in orange and those synchronized with CO peaks are shown in red. (c) Experimental CO_2 production obtained on the sputter-annealed Pt/TiO_2(110)-(1×1) model catalyst whose an STM image is shown in Figure S3b.*

The coupled differential equations 1 and 2 have been solved numerically and the resulting CO and O coverages are shown as a function of temperature and time in Figure S4a in green and blue, respectively. The CO_2 production is calculated within the mean-field approximation[11] assuming a

random distribution of the reactants on the surface, and therefore it is proportional to the product of the simulated CO and O coverages. The CO_2 production synchronized with CO pulses is represented in red in Figure S4b and the one synchronized with oxygen pulses in orange.

Figures S4a and b clearly reveal the transition from CO poisoning,[12] where oxygen can not dissociate due to a monolayer of chemisorbed CO molecules, to an oxygen-rich regime where the reaction rate is limited by CO. Between 350 and 450 K both regimes overlap and CO_2 is produced at pulses of each of the two reactants. Comparison between Figures S4b and c shows that the simulations agree quantitatively with experiment; only the O_2-related CO_2 production spans a wider temperature interval in the simulations. The fact that the binding energies that produced this agreement are typical values for Pt(111) reveals that the Pt clusters on TiO_2(110)-(1×1) are representative of clean Pt surfaces.

References

(1) (a) Vandoni, G.; Félix, C.; Monot, R.; Buttet, J.; Harbich, W. *Chem. Phys. Letters* **1994**, *229*, 51. (b) Bonanni, S.; Aït-Mansour, K.; Hugentobler, M.; Brune, H.; Harbich, W. *Eur. Phys. J. D*, in press.

(2) Horcas, I.; Fernández, R.; Gómez-Rodríguez, J. M.; Colchero, J.; Gómez-Herrero, J.; Baro, A. M. *Rev. Sci. Instrum.* **2007**, *78*, 013705.

(3) Diebold, U. *Surf. Sci. Rep.* **2003**, *48*, 53 and references therein.

(4) (a) Henderson, M. A. *Langmuir* **1996**, *12,* 5093. (b) Henderson, M. A.; Epling, W. S.; Perkins, C. L.; Peden, C. H. F.; Diebold, U. *J. Phys. Chem. B* **1999**, *103,* 5328.

(5) Hugenschmidt, M. B.; Gamble, L.; Campbell, C. T. *Surf. Sci.* **1994***, 302,* 329.

(6) (a) Zhang, Z.; Bondarchuk, O.; Kay, B. D.; White, J. M.; Dohnálek, Z. *J. Phys. Chem. B* **2006,** *110,* 21840. (b) Wendt, S.; Schaub, R.; Matthiesen, J.; Vestergaard, E. K.; Wahlström, E.; Rasmussen, M. D.; Thostrup, P.; Molina, L. M.; Lægsgaard, E.; Stensgaard, I.; Hammer, B.; Besenbacher, F. *Surf. Sci.* **2005**, *598*, 226. (c) Li, S.-C.; Zhang, Z.; Sheppard, D.; Kay, B. D.; White, J. M.; Du, Y.; Lyubinetsky, I.; Henkelman, G.; Dohnálek, Z. *J. Am. Chem. Soc.* **2008**, *130*, 9080.

(7) (a) Wendt, S.; Sprunger, P. T.; Lira, E.; Madsen, G. K. H.; Li, Z.; Hansen, J. Ø.; Matthiesen, J.; Blekinge-Rasmussen, A.; Lægsgaard, E.; Hammer, B.; Besenbacher, F. *Science* **2008**, *320*, 1755. (b) Yim, C. M., Pang, C. L.; Thornton, G. *Phys. Rev. Lett.* **2010**, *104*, 036806.

(8) Zhang, Z.; Lee, J.; Yates, J. T.; Jr.; Bechstein, R.; Lira, E.; Hansen, J. Ø.; Wendt S.; Besenbacher, F. *J. Phys. Chem. C* **2010,** *114,* 3059.

(9) (a) Brinkley, D.; Dietrich, M.; Engel, T.; Farrall, P.; Gantner, G.; Schafer, A.; Szuchmacher, A. *Surf. Sci.* **1998**, *395,* 292. (b) Dohnálek, Z.; Kim, J.; Bondarchuk, O.; White, J. M.; Kay, B. D. *J. Phys. Chem. B* **2006**, *110,* 6229.

(10)(a) Verheij, L. K.; Lux, J.; Anton, A. B.; Poelsema, B.; Comsa, G. *Surf. Sci.* **1987**, *182,* 390. (b) Winkler, A.; Guo, X.; Siddiqui, H. R.; Hagans, P. L.; Yates Jr.; J. T. *Surf. Sci.* **1988**, *201,* 419. (c) Shan, B.; Zhao, Y.; Hyun, J.; Kapur, N.; Nicholas, J. B.; Cho, K. *J. Phys. Chem. C* **2009,** *113,* 6088.

(11)Wintterlin, J.; Völkening, S.; Janssens, T. V. W.; Zambelli, T.; Ertl, G. *Science* **1997**, *278*, 1931.

(12)(a) Campbell, C. T.; Ertl, G.; Kuipers, H.; Segner, J. *J. Chem. Phys.* **1980**, *73*, 5862. (b) Engel, T.; Ertl, G. *Chem. Phys. Lett.* **1978**, *54*, 95. (c) Engel, T.; Ertl, G. *J. Chem. Phys.* **1978**, *69*, 1267. (d) Conrad, H.; Ertl, G.; Küppers, J. *Surf. Sci.* **1978**, *76*, 323. (e) Kunz, S.; Schweinberger, F. F.; Habibpour, V.; Röttgen, M.; Harding, C.; Arenz, M.; Heiz, U. *J. Phys. Chem. C* **2010**, *114*, 1651.